SCIENTIFIC REPORTS

OPEN

SUBJECT AREAS:
QUANTUM OPTICS
NONLINEAR OPTICS

Received
3 September 2013

Accepted
12 December 2013

Published
9 January 2014

Correspondence and requests for materials should be addressed to Y.P.Z. (ypzhang@mail.xjtu.edu.cn) or M.X. (mxiao@uark.edu)

Parametrically Amplified Bright-state Polariton of Four- and Six-wave Mixing in an Optical Ring Cavity

Haixia Chen[1], Yiqi Zhang[1], Xin Yao[1], Zhenkun Wu[1], Xun Zhang[1], Yanpeng Zhang[1] & Min Xiao[2]

[1]Key Laboratory for Physical Electronics and Devices of the Ministry of Education & Shaanxi Key Lab of Information Photonic Technique, Xi'an Jiaotong University, Xi'an 710049, China, [2]Department of Physics, University of Arkansas, Fayetteville, Arkansas 72701, USA & National Laboratory of Solid State Microstructures and Department of Physics, Nanjing University, Nanjing 210093, China.

We report experimental studies of bright-state polaritons of four-wave mixing (FWM) and six-wave mixing (SWM) signals through cascade nonlinear optical parametric amplification processes in an atom-cavity composite system for the first time. Also, the coexisting cavity transmission modes of parametrically amplified FWM and SWM signals are observed. Finally, electromagnetically induced absorption by the FWM cavity modes in the probe beam is investigated. The investigations can find potential applications in multi-channel narrow-band long-distance quantum communication.

Cavity quantum electrodynamics has been intensively studied in recent years[1–4], owing to the important applications in quantum optics and nonlinear optics. When a two-level atom is placed inside the optical cavity under the strong coupling condition, the "normal-mode splitting" have been experimentally demonstrated in many atomic systems. If the intracavity medium is a coherently-prepared three-level atomic medium, the so called "dark-state polariton" peak[5–7] appears in the cavity transmission spectrum (CTS) due to the intracavity electromagnetically induced transparency (EIT). Such "dark-state polariton" have potential application in the long-lived storage of quantum information and quantum computation. Moreover, when the atomic system is in the double-Λ configuration, correlated photon pairs with high generation rate and narrow bandwidth have been generated[8] in the cold atomic ensemble by using an optical parametric amplification (OPA) process operated below its oscillation threshold. Meanwhile, bright correlated anti-Stokes and Stokes twin beams with hot atoms inside an optical cavity have also been obtained by an OPA process above the threshold[9]. When an ensemble of cold atoms strongly coupled to a high-finesse optical cavity, and the control light can be generated from the vacuum, then the vacuum-induced transparency was observed[10]. In addition, four-wave mixing (FWM) and six-wave mixing (SWM) processes based on third-order and fifth-order nonlinear processes in EIT media[11–13] have also attracted lots of attention in recent years, in which a strong coupling beam renders a resonant, opaque medium nearly transparency while enhancing the nonlinearity, and the coexistence of these two nonlinear processes due to double EIT windows and atomic coherences has been reported[14,15]. The nonlinear process plays important role in entanglement generation[16,17] and cascade-nonlinear optical process[18]. To the best of our knowledge, the OPA seeded with FWM or SWM signal in an atom-cavity composite system has not been reported, and the investigation of it would be important for building multi-channel nonlinear optical devices and ultra-narrow linewidth photon sources for long-distance quantum communication[19].

In this letter, we report our investigations of bright-state polaritons of FWM and SWM signals through cascade OPA process in an atom-cavity composite system. The bright-state polaritons of FWM signal with 5 MHz linewidth are obtained. We also report the coexisting cavity modes of parametrically amplified FWM and SWM signals in an inverted-Y-type atomic system for the first time. Moreover, the electromagnetically induced absorption (EIA) peaks induced by the multiple cavity modes of the FWM signal are observed in the probe beam. These results are well explained by the presented theoretical model. The investigation will help us to better understand the interactions between the strongly coupled multi-level atoms and the optical cavity, which can find application in quantum information processing.

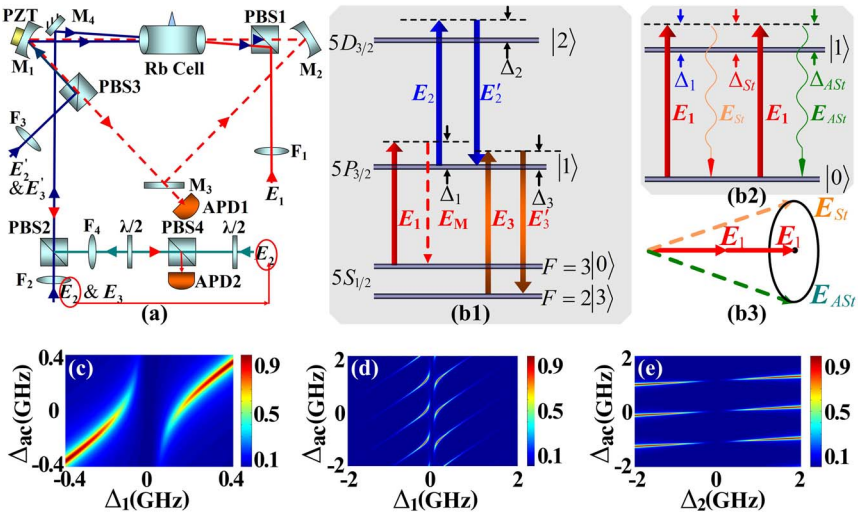

Figure 1 | (a) Experimental setup. PBS: polarizing beam splitters; F: optical lens; APD: avalanche photodiode detectors; PZT: piezoelectric transducer; M1–M3: cavity mirrors; M4, high reflectivity mirror; $\lambda/2$: half-wave plate. (b1) Energy levels for the ^{85}Rb atomic system. (b2) Energy schematic of SP-FWM process. (b3) phase-matching geometrical diagram of SP-FWM process. Calculated CTS versus Δ_1 and Δ_{ac} by using the expression of a_{F1} (c) in a FSR and (d) in multiple FSRs. (e) Calculated CTS versus Δ_2 and Δ_{ac} by using the expression of a_{F1} in multiple FSRs.

Results

Fig. 1(a) shows the experimental setup, while the energy levels of the atomic system used in the experiment is shown in Fig. 1(b1), where the fields $\boldsymbol{E}_1$ (frequency ω_1, wave vector $\boldsymbol{k}_1$, Rabi frequency G_1, and wavelength 780.2 nm), $\boldsymbol{E}_2$ (ω_2, $\boldsymbol{k}_2$, G_2, and 776.16 nm) & $\boldsymbol{E}'_2$ (ω_2, $\boldsymbol{k}'_2$, G'_2), and $\boldsymbol{E}_3$ (ω_3, $\boldsymbol{k}_3$, G_3, and 780.2 nm) & $\boldsymbol{E}'_3$ (ω_3, $\boldsymbol{k}'_3$, G'_3) are used as probe field, pumping fields and coupling fields, respectively. The resonant transition frequencies of $|0\rangle\rightarrow|1\rangle$, $|1\rangle\rightarrow|2\rangle$ and $|1\rangle\rightarrow|3\rangle$ are Ω_1, Ω_2 and Ω_3, respectively. Then the frequency detuning for each field can be defined as $\Delta_i = \Omega_i - \omega_i$ (i = 1, 2, 3). With all beams present in Fig. 1(b1), three phase-conjugate signals (FWM signals $\boldsymbol{E}_{F1}$ & $\boldsymbol{E}_{F2}$ and SWM signal $\boldsymbol{E}_S$), satisfying the phase-matching conditions of $\mathbf{k}_{F1}=\mathbf{k}_1+\mathbf{k}_2-\mathbf{k}'_2$, $\mathbf{k}_{F2}=\mathbf{k}_1+\mathbf{k}_3-\mathbf{k}'_3$, and $\mathbf{k}_S=\mathbf{k}_1+\mathbf{k}_2-\mathbf{k}_2+\mathbf{k}_3-\mathbf{k}'_3$, can be generated simultaneously at the center of the atomic cell and propagate along the optical axis of the cavity (dashed line in Fig. 1(a)). Here, the narrow signals $\boldsymbol{E}_{F1}$ and $\boldsymbol{E}_S$ are generated within the EIA window of $\delta = 0$, where $\delta = \Delta_1 + \Delta_2$ is two-photon detuning, while the broad signal $\boldsymbol{E}_{F2}$ will be generated due to no assistance of Doppler-free atomic coherence and EIA window. However, if the $\boldsymbol{E}_1$ beam has a sufficiently high power, as well as is far detuned from $|0\rangle\rightarrow|1\rangle$, a spontaneous parametric FWM (SP-FWM) process will occur in the degenerate two-level atomic configuration (Fig. 1(b2)), which generates two weak fields (Stokes field $\boldsymbol{E}_{St}$ and anti-Stokes field $\boldsymbol{E}_{ASt}$), satisfing $2\mathbf{k}_1 = \mathbf{k}_{St} + \mathbf{k}_{ASt}$ (Fig. 1(b3)), on a forward cone. The generated $\boldsymbol{E}_{F1}$ (or $\boldsymbol{E}_S$) signal is naturally injected into the input Stokes port of the SP-FWM process, and is parametrically amplified, where the process will serve as an OPA. The parametrically amplified signal denoted as $\boldsymbol{E}^A_{F1}$ (or $\boldsymbol{E}^A_S$) is still generated at the center of the atomic cell and propagate along the optical axis of the cavity, so they are mode-matched to the cavity and form the cavity modes.

According to the expression of a_{F1} given in the Method part, Fig. 1(c) shows the calculated normalized CTS versus Δ_{ac} (defined as $\Delta_{ac} = \Omega_1 - \omega_c$ with ω_c being the resonant frequency of the cavity) and Δ_1, which exhibits a double-peak structure along the Δ_1 direction. This structure indicates the cavity polaritons[7] of the parametrically amplified field $\boldsymbol{E}^A_{F1}$, which results from the coupling between the cavity mode of $\boldsymbol{E}^A_{F1}$ and atoms with strength $g\sqrt{N}$, where g is the single-atom-cavity coupling strength, and N is the number of atoms in the cavity. When Δ_{ac} changes from negative to positive continuously, the polaritons move, that is dictated by the condition of $\Delta_1 - \Delta_{ac} = 0$, and finally leads to the avoided-crossing plot in Fig. 1(c). Fig. 1(d) is plotted with the same variables as Fig. 1(c) but in a wider range, where multiple polaritons at a fixed Δ_1 can be seen, and their positions change as Δ_1 changes. It is found that $\Delta_{F1} - \Delta_{ac} = l\omega_{FSR}$ (l is an integer, and ω_{FSR} is the free-spectral range (FSR) with medium) is always fulfilled at all the polaritons, i.e. $\Delta_1 - \Delta_{ac} = l\omega_{FSR}$ (named cavity transmission window) is satisfied for all the polaritons. So, when Δ_1 changes, the corresponding Δ_{ac} for each transmission polaritons of $\boldsymbol{E}^A_{F1}$ changes accordingly. We also show normalized CTS versus Δ_2 and Δ_{ac} in Fig. 1(e), in which the polaritons nearly do not move with Δ_2. The reason is that the energy shifts induced by dressing field $\boldsymbol{E}_2$ at different Δ_2 values make the window $\Delta_1 - \Delta_{ac} = l\omega_{FSR}$ not move.

It is worth mentioning that the cavity polaritons of the parametrically amplified field $\boldsymbol{E}^A_{F1}$ and $\boldsymbol{E}^A_S$ will have ultra-narrow linewidths, which would be useful for long-distance quantum communications. On the one hand, the linewidths of $\boldsymbol{E}^A_{F1}$ and $\boldsymbol{E}^A_S$ are narrowed by the EIA window, on the other hand, $\boldsymbol{E}^A_{F1}$ and $\boldsymbol{E}^A_S$ form cavity modes, and then the cavity polaritons will be further narrowed due to the large dispersion change and reduced absorption accompanying EIA[20,21].

Parametrically amplified bright-state polariton of FWM signal. We first measure the CTS without $\boldsymbol{E}_3$ and $\boldsymbol{E}'_3$. In this case, the SP-FWM process generates a Stokes field $\boldsymbol{E}_{St}$ (measured and shown in Fig. 2(a1)) and an anti-Stokes field $\boldsymbol{E}_{ASt}$ (measured and shown in Fig. 2(a2)) on a forward cone. Such a process can also act as an OPA for the $\boldsymbol{E}_{F1}$ (in Fig. 2(a3)) injected into the Stokes port (in Fig. 2(a4)). The parametrically amplified signal denoted as $\boldsymbol{E}^A_{F1}$ forms cavity mode, which couples with the atoms. By scanning Δ_1 across the transition $F = 3\leftrightarrow F'$ in ^{85}Rb at different Δ_{ac} values and taking $\Delta_2 \approx 1.2$ GHz, the measured CTS of $\boldsymbol{E}^A_{F1}$ versus δ are shown in Figs. 2(b1)–(b3), where the lower curves (ii) and top curves (i) are the CTS of $\boldsymbol{E}^A_{F1}$ and the corresponding EIA window, respectively, with the atomic cell temperature $T \approx 77^\circ$C, and powers of $\boldsymbol{E}_1$, $\boldsymbol{E}_2$, and $\boldsymbol{E}'_2$ $P_1 = 8$ mW, $P_2 = 22$ mW, $P'_2 = 22$ mW, respectively. The CTS of $\boldsymbol{E}^A_{F1}$ without the atom-cavity mode coupling is shown in Fig. 2(b2) by the curve (iii), where one dip and two peaks can be seen clearly. The two peaks represent the Autler-Townes splitting of the signal $\boldsymbol{E}^A_{F1}$, which derive from the two dressed states, namely, bright states. The dip comes from the dark state induced by the destructive interference between two dressed states. Tuning Δ_{ac}

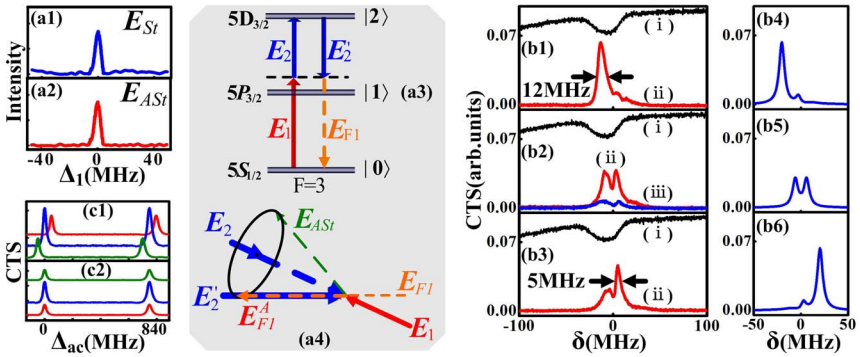

Figure 2 | (a1) Measured Stokes field $\boldsymbol{E}_{St}$ and (a2) anti-Stokes field $\boldsymbol{E}_{ASt}$ versus Δ_1 in the SP-FWM process. (a3) Ladder-type atomic levels to generate $\boldsymbol{E}_{F1}$. (a4) Phase-matching diagram of OPA seeded with the $\boldsymbol{E}_{F1}$ in the Stokes port. (b1)–(b3) Measured probe absorption (i) and CTS (ii) versus δ at different Δ_{ac}. (b4)–(b6) Theoretical simulation of the curves (ii) in Figs. (b1)–(b3), respectively. (c1) and (c2) Measured polaritons of $\boldsymbol{E}_{F1}^A$ versus Δ_{ac} with increasing Δ_1 and Δ_2 from bottom to top, respectively.

with the atom-cavity mode coupling indicates that, when the $\Delta_1 - \Delta_{ac} = 0$ window is overlapped with the EIA window, the two peaks reach their maxima simultaneously on the curve (ii) of Fig. 2(b2). Comparing the curve (iii) with the curve (ii), the dip (corresponding to dark state) and the two peaks is amplified, which stems from the dressing splitting of the atom-cavity mode coupling to the energy level $|1\rangle$. So the two peaks on the curve (ii) represent the cavity polaritons of $\boldsymbol{E}_{F1}^A$ as shown in Fig. 1(c). When the $\Delta_1 - \Delta_{ac} = 0$ window deviates from EIA window by decreasing Δ_{ac}, the two peaks become asymmetric, and the left peak is amplified by the atom-cavity mode coupling as shown in Fig. 2(b1). The left peak corresponds to one of the bright states, so one intracavity bright state ("bright-state polariton" with a linewidth about 12 MHz) is obtained. The other narrow "bright-state polariton" (~5 MHz) is obtained when increasing Δ_{ac} in Fig. 2(b3). The calculated CTS curves of $\boldsymbol{E}_{F1}^A$ ($\propto |a_{F1}|^2$), which agree well with the measured results, are shown in Figs. 2(b4)–2(b6).

By scanning the voltage imposed on PZT, Fig. 2(c1) displays the parametrically amplified bright-state polaritons of $\boldsymbol{E}_{F1}^A$ versus Δ_{ac} at different δ values, which is set as −12 MHz, 0 and 12 MHz from bottom to top by taking different Δ_1 with fixed Δ_2. Each CTS curve exhibits two bright polaritons, satisfying $\Delta_1 - \Delta_{ac} = l\omega_{FSR}$, having a separation of ω_{FSR}, and changing their positions with Δ_1 as predicted by the theoretical result in Fig. 1(d). Also, the heights of the polaritons change with Δ_1, since the polaritons are enhanced at two-photon resonant. Next, by fixing Δ_1 and taking different Δ_2, the bright-state polaritons of $\boldsymbol{E}_{F1}^A$ versus Δ_{ac} with δ set as −15 MHz, 0 and 15 MHz from bottom to top are shown in Fig. 2(c2), where the heights of the polaritons change with Δ_2 due to two-photon detuning, but the positions are fixed. That is similar to the case shown in Fig. 1(e).

The polaritons of $\boldsymbol{E}_{F1}^A$ can be affected by the temperature of atomic cell, since increasing T can increase the atomic number N, and then enlarge the collective coupling factor $g\sqrt{N}$, which will yield dressing to the polaritons. According to the theoretical model presented in the method part, the splitting eigenvalues induced by the dressing of atom-cavity mode coupling to the polaritons can be given by $\lambda_{1,2} = \left(-\Delta_1 \pm \sqrt{\Delta_1^2 + 4g^2N}\right)\Big/2$, which correspond to the positions of the two polariton peaks in the CTS curves. So the splitting of the two polariton peaks will increase with T. Also, increasing temperature will lead to increased atomic number participating in the phase-conjugate FWM process as well as OPA process, which will enhance the height of the two polariton peaks. The measured CTS curves versus δ with increasing T from bottom to top are shown in Fig. 3(a1), where not only the height but also the splitting of the two polariton peaks increase with T. Fig. 3(A1) shows the calculated results corresponding to Fig. 3(a1), according to the expression of a_{F1}. The experimentally measured (squares) and theoretically calculated (solid line) splittings of polaritons versus T are shown in Fig. 3(a2), where the splitting indeed increases with T. The experimental results agree with the theory.

The polaritons of $\boldsymbol{E}_{F1}^A$ can also be influenced by the powers P_1 and P_2. The measured CTS curves versus δ with increasing P_2 from bottom to top are presented in Fig. 3(b1). The height and the splitting of the two polariton peaks become more pronounced as P_2 increase. Figure 3(b2) shows the splitting versus P_2 with the atom-cavity mode coupling (upper plots) and without the atom-cavity mode coupling (lower plots), where squares and dots are experimental results, while the solid curves are the corresponding fittings. The splitting on upper plots in Fig. 3(b2) is mainly induced by the dressing of the atom-cavity mode coupling and field $\boldsymbol{E}_2$ to polaritons, while the splitting on lower plots mainly results from the dressing of the field $\boldsymbol{E}_2$. By comparing the two cases, the dressing splitting of the atom-cavity mode coupling can be obtained. While the dressing splitting induced by field $\boldsymbol{E}_2$ to the polariton can be seen by increasing P_2. Similar investigation has been done for the influence of P_1 in Figs. 3(c1) and 3(c2). However, the upper squares (or solid line) in Fig. 3(c2) is much easier to saturate than that in Fig. 3(b2). The dressing splitting of the polariton in Fig. 3(c2) is mainly determined by the atom-cavity coupling and field $\boldsymbol{E}_2$ when the power of P_1 is weak, which is similar to the case in Fig. 3(b2). As P_1 is increased, the dressing of field $\boldsymbol{E}_1$ gets larger and has to be considered. So the dressing splitting of field $\boldsymbol{E}_1$ to polaritons is included in Fig. 3(c2) compared with Fig. 3(b2). Therefore, the saturation behavior with increasing P_1 in Fig. 3(c2) mainly results from the balanced interactions between the destructive and constructive interferences of different dressing pathways[22] induced by the atom-cavity mode coupling, field $\boldsymbol{E}_1$ and field $\boldsymbol{E}_2$.

Coexisting cavity modes of parametrically amplified FWM and SWM signals. If all laser beams are opened except $\boldsymbol{E}_2'$ (Fig. 1(b1)), we can get an inverted Y-type system, in which there will be $\boldsymbol{E}_S$ and $\boldsymbol{E}_{F2}$ but no $\boldsymbol{E}_{F1}$. As indicated by Fig. 4(f), $\boldsymbol{E}_S$ signal is naturally used as a seed injected into the Stokes port of SP-FWM process and amplified as $\boldsymbol{E}_S^A$. Then, the $\boldsymbol{E}_S^A$ signal, mode-matched to the cavity, forms a cavity mode. In free space, the measured coexisting spectrum of $\boldsymbol{E}_S^A$ and $\boldsymbol{E}_{F2}$ versus δ with $\Delta_2 = 1.2$ GHz is displayed as the bottom curve in the inset of Fig. 4(a), in which a narrow peak labeled as "S" (corresponding to EIA dip labeled as "E" on the top curve) and a broad signal can be seen. The frequency of peak "S" changes with Δ_2, so peak "S" is the signal $\boldsymbol{E}_S^A$, while the broad signal is $\boldsymbol{E}_{F2}$ without the EIA window. With both $\boldsymbol{E}_S^A$ and $\boldsymbol{E}_{F2}$ resonant in the cavity, the measured CTS versus δ is given by the bottom solid curve in Fig. 4(a), where we can see five peaks labeled as "P1", "P2", "ST"

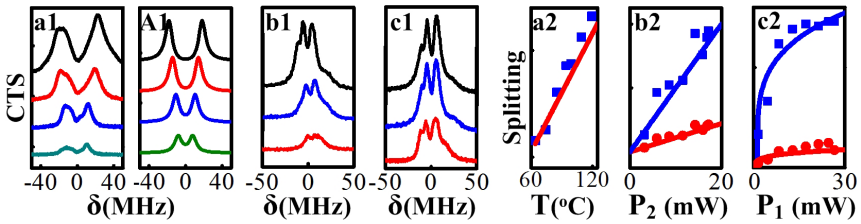

Figure 3 | (a1) Measured polaritons of the E_{F1}^{A} versus δ with $\Delta_2 \approx 1.2$ GHz and increasing T from bottom to top (65°C, 75°C, 85°C, 95°C). (A1) Theoretical simulation of the curves in (a1). (a2) Measured (squares) and Calculated (solid line) dressing splittings versus T. (b1) Measured polaritons with increasing P_2 from bottom to top (3.3 mW, 8.6 mW, 17 mW). (b2) P_2-dependence of the splitting with (top curves) and without (bottom curves) atom-cavity mode coupling. (c1) and (c2) are plotted in the same way as (b1) and (b2) but with increasing P_1 (2.5 mW, 6 mW, 12 mW).

"P3", and "P4", respectively, and the peak "ST" corresponds to the EIA dip "E" on the top dash-dotted curve. Without E_2, both the "ST" peak and "E" dip disappear in Fig. 4(b). So we can identify the "ST" peak is the transmission peak of E_S^A, and the other four peaks are the cavity modes of E_{F2} picked out by the cavity windows from the broad gain. Tuning the cavity length to make a cavity transmission peak of E_{F2} overlap with the "ST" peak (i.e. the cavity window overlaps with the EIA window), the resulted CTS (the solid curve) and the corresponding EIA (the dash-dotted curve) versus δ are shown in Fig. 4(c), where the coexisting cavity modes of the SWM (E_S^A) and FWM (E_{F2}) signals are obtained. By blocking E_2 at this time, the cavity mode of the SWM signal disappears, and only the cavity modes of E_{F2} survive (dashed line of Fig. 4(c)). Comparing the results with and without E_2 in Fig. 4(c), the enhancement (bright-state polariton of E_S^A) due to the coupling of cavity mode of E_S^A with atoms can be seen. Also, the pulling of the cavity resonant frequency due to the dispersion change induced by E_2[20,21] can be observed. By fixing Δ_1 and Δ_2 at the point of coexisting cavity modes and scanning Δ_{ac} in Fig. 4(d), the measured coexisting cavity modes of E_S^A and E_{F2} versus Δ_{ac} are shown on the solid curve, while the dashed curve shows the cavity modes of E_{F2} without E_2. Also, the pulling of the cavity resonant frequency is observed in Fig. 4(d). According to the coupled atom-cavity model, the CTS amplitude of E_S^A is given by $a_S = T_c G_S^A \rho_{00} / \{[i(\Delta_S - \Delta_{ac}) + \gamma] + g^2 N / (d_1 + |G_2|^2/d_2 + |G_3|^2/d_3)\}$, where $\Delta_S = \Omega_1 - \omega_S$, $d_3 = \Gamma_{30} + i(\Delta_1 - \Delta_3)$, and G_S^A is the Rabi frequency of E_S^A. The transmission coefficient of intensity of E_{F2} is $T_{F2} = (t_2 t_3)^2 e^{-\alpha L_a} / \left[\left(1 - r_2 r_3 e^{-\alpha L_a/2}\right)^2 + 4 r_2 r_3 e^{-\alpha L_a/2} \sin^2(\phi/2) \right]$, where r_i (t_i) is the reflection (transmission) coefficient of the mirror M_i of the cavity with $r_i^2 + t_i^2 = 1$, and $\phi(\omega_{F2}) = 2\pi(\Delta_{ac} - \Delta_1)/\omega_{FSRE} + (n-1)L_a\omega_{F2}/c$ is the round-trip phase shift experienced by E_{F2}, with light speed in vacuum c, length of the atomic cell L_a, and FSR of the empty optical cavity $\omega_{FSRE} = c/L_c$ with a cavity length L_c. The terms $\alpha = 2(\omega_{F2}/c)\mathrm{Im}[(1+\chi)^{1/2}]$ and $n = \mathrm{Re}[(1+\chi)^{1/2}]$ are the intensity absorption coefficient and refractive index of the atomic medium, respectively, with $\chi = i2g^2 N L_c / [L_a \omega_{F2}(d_1 + |G_2|^2/d_2 + |G_3|^2/d_3)]$ when only the linear susceptibility is considered. Using the expressions of a_S and T_{F2}, the calculated normalized CTS of coexisting E_S^A and E_{F2} versus δ are shown on the bottom curve in Fig. 4(e), which agrees with the experimental result.

Besides, the EIA peaks induced by the multiple cavity modes of E_{F2} are observed in Fig. 4(b), where each inset is a measured EIA peak multiplied by 10. Because each cavity mode of E_{F2} couples to $|0\rangle \rightarrow |1\rangle$ and propagates along the same direction as E_1, the two-photon resonance (one photon from E_1 and another from E_{F2}) induces the Doppler-free atomic coherence[23]. Owing to the far detuning of the cavity modes of E_{F2}, the EIA is induced instead of EIT. The probe absorption can be obtained by $\rho_{10}^{(1)} = iG_1 \Big/ \Big\{ d_1 + |G_2|^2/d_2 + |G_{F1}^A|^2 / d_{F1} + |G_{F2}|^2/d_{ac} + |G_S^A|^2 \Big/ d_S \Big\}$ with $d_{F1} = i(\Delta_1 - \Delta_{F1}) + \Gamma_{10}$, $d_{ac} = i(\Delta_1 - \Delta_{ac}) + \Gamma_{10}$ and $d_S = i(\Delta_1 - \Delta_S) + \Gamma_{10}$, which indicates E_2 field and the cavity modes of E_{F1}^A&E_S^A&E_{F2} with far detuning can all induce EIA. However, the induced EIA by the cavity modes of E_{F1}^A&E_S^A are not easy to be observed separately, because they overlap with the EIA created by the E_2 field, which is much stronger than the cavity modes. The induced EIA (insets of Fig. 4(b)) by the cavity modes of E_{F2} can be observed by tuning Δ_{ac} or Δ_2 to separate it from the EIA of E_2. The calculated probe absorption by $\rho_{10}^{(1)}$ is shown on the top curve in Fig. 4(e), where the highest EIA peak is the sum from

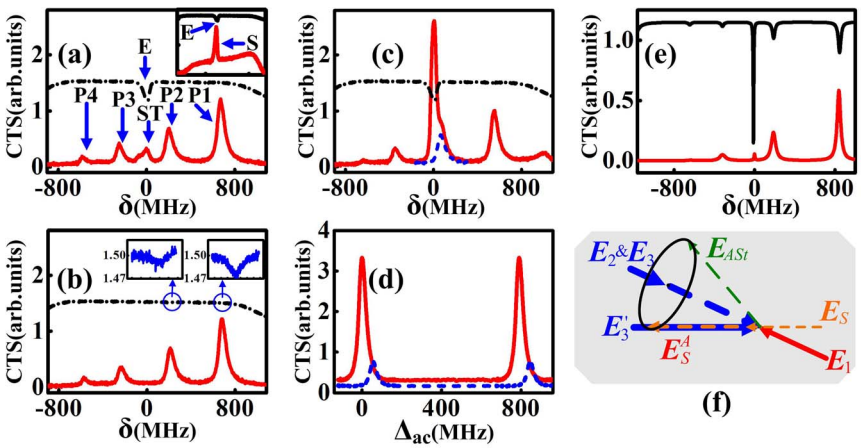

Figure 4 | (a)–(c) Measured CTS of E_{F2} and E_S^A signals versus δ at different Δ_{ac} values. Coexisting E_S^A and E_{F2} signals versus δ in free space shown in the inset of (a), and measured FWM-induced EIA dips shown in the insets of (b). (d) Measured CTS of E_{F2} and E_S^A signals versus Δ_{ac} with (solid curve) and without (dashed curve) E_2. (e) Calculated FWM-induced EIA (top curve) and CTS (bottom curve) with coexisting E_{F2} and E_S^A versus δ. (f) Phase-matching of OPA process seeded with E_S.

$\boldsymbol{E}_2$ and cavity modes of $\boldsymbol{E}_{F1}^A$ &$\boldsymbol{E}_S^A$, and the other peaks are induced by the cavity modes of $\boldsymbol{E}_{F2}$.

Discussion

We have experimentally studied the bright-state polaritons of multi-wave mixing signals through OPA processes in a multi-level atom-cavity composite system. It is demonstrated that the polaritons are much narrowed due to EIA and cavity window. It would be important for the narrow-band long-distance quantum communications. Besides, coexisting cavity modes of the generated SWM and FWM signals are also observed, which can help us to better understand the interactions between the strongly coupled multi-level atoms and the optical cavity. Moreover, the induced EIA by the multiple FWM cavity modes in the probe spectrum is observed. Such investigation in an atom-cavity coupling system may find potential applications in building multi-channel nonlinear optical devices for quantum information processing.

Methods

Experiment setup. The atom-cavity composite system is shown in Fig. 1(a), where a 7 cm long Rb atomic cell is placed inside a 38 cm long optical ring cavity. The concave mirrors M1 and M2 (with the same radius of curvature of 100 mm) have 99.9% and 97.5% reflectivities at 780 nm, respectively. The flat mirror M3 with a reflectivity of 97.5% at 780 nm is used as the output coupler. M1 is mounted on a piezoelectric transducer (PZT) to adjust and lock the cavity length. The atoms can be viewed as an inverted four-level Y-type system as shown in Fig. 1(b1), where the relevant energy levels are $5S_{1/2}(F=3)(|0\rangle)$, $5P_{3/2}(|1\rangle)$, $5D_{3/2}(|2\rangle)$ and $5S_{1/2}(F=2)(|3\rangle)$ in ^{85}Rb. Three grating-stabilized diode lasers are used as the probe field $\boldsymbol{E}_1$ (frequency ω_1, wave vector $\boldsymbol{k}_1$, Rabi frequency G_1, and wavelength 780.2 nm), pumping fields $\boldsymbol{E}_2$ (ω_2, $\boldsymbol{k}_2$, G_2, and 776.16 nm) & $\boldsymbol{E}_2'$ (ω_2, $\boldsymbol{k}_2'$, G_2'), and coupling fields $\boldsymbol{E}_3$ (ω_3, $\boldsymbol{k}_3$, G_3, and 780.2 nm) & $\boldsymbol{E}_3'$ (ω_3, $\boldsymbol{k}_3'$, G_3'), where $\boldsymbol{E}_1$ drives the transition $|0\rangle\rightarrow|1\rangle$, $\boldsymbol{E}_2$ & $\boldsymbol{E}_2'$ drive $|1\rangle\rightarrow|2\rangle$, and $\boldsymbol{E}_3$ & $\boldsymbol{E}_3'$ drive $|1\rangle\rightarrow|3\rangle$. The $\boldsymbol{E}_2$ (with horizontal polarization) and $\boldsymbol{E}_2'$ (with vertical polarization) beams come from the same laser. $\boldsymbol{E}_2'$ beam propagates along the optical axis of the cavity, and $\boldsymbol{E}_2$ beam co-propagates with $\boldsymbol{E}_2'$ beam having a 2° angle between them. The $\boldsymbol{E}_1$ (vertically polarized) beam counter-propagates with $\boldsymbol{E}_2$ beam; that is the two-photon Doppler-free scheme for ladder-type system[23]. The CTS and absorption of $\boldsymbol{E}_1$ is detected by avalanche photodiode detector 1 (APD1) and APD2, respectively. The $\boldsymbol{E}_3$ and $\boldsymbol{E}_3'$ beams have the same propagation directions and polarizations with $\boldsymbol{E}_2$ and $\boldsymbol{E}_2'$ beams, respectively.

Theoretical model. According to the perturbation chains[15], the density-matrix elements for $\boldsymbol{E}_{F1}$ and $\boldsymbol{E}_S$ are $\rho_{10}^{(3)}=-iG_1G_2G_2'^{*}\exp(i\mathbf{k}_{F1}\cdot\mathbf{r})/\left[d_2(d_1+G_2/d_2)^2\right]$ and $\rho_{10}^{(5)}=iG_1G_2G_2^{*}G_3G_3^{*}\exp(i\mathbf{k}_S\cdot\mathbf{r})/\left(d_1^3d_2d_3\right)$, where $d_1=\Gamma_{10}+i\Delta_1$, $d_2=\Gamma_{20}+i(\Delta_1+\Delta_2)$ and $d_3=\Gamma_{30}+i(\Delta_1-\Delta_3)$ with the decay rate Γ_{ij} between states $|i\rangle$ and $|j\rangle$. The generated $\boldsymbol{E}_{F1}$ (or $\boldsymbol{E}_S$) signal is injected into the Stokes port of the SP-FWM process, then parametrically amplified and denoted as $\boldsymbol{E}_{F1}^A$ (or $\boldsymbol{E}_S^A$). The photon numbers of the output Stokes ($\boldsymbol{E}_{F1}^A$ or $\boldsymbol{E}_S^A$) and anti-Stokes fields of the OPA are $\langle\hat{a}_{out}^{+}\hat{a}_{out}\rangle=G\langle\hat{a}_{in}^{+}\hat{a}_{in}\rangle+(G-1)$ and $\left\langle\hat{b}_{out}^{+}\hat{b}_{out}\right\rangle=(G-1)\langle\hat{a}_{in}^{+}\hat{a}_{in}\rangle+(G-1)$, where $\hat{a}\left(\hat{b}\right)$ is the annihilation operator of $\boldsymbol{E}_{St}$ ($\boldsymbol{E}_{ASt}$), and $G=\left\{\cos\left[2t\sqrt{AB}\sin(\varphi_1+\varphi_2)/2\right]+\cosh\left[2t\sqrt{AB}\cos(\varphi_1+\varphi_2)/2\right]\right\}/2$ is the gain of the process with the modules A and B (phases φ_1 and φ_2) defined in $\rho_{10(S)}^{(3)}=Ae^{i\varphi_1}$ and $\rho_{10(ASt)}^{(3)}=Be^{i\varphi_2}$ for $\boldsymbol{E}_{St}$ and $\boldsymbol{E}_{ASt}$, respectively[18].

Then, we describe the theoretical model of such coupled atom-cavity system. Here, we just discuss the model with the cavity mode of $\boldsymbol{E}_{F1}^A$ coupling with atoms, since the case for $\boldsymbol{E}_S^A$ can be discussed in the same way. In the limit of weak cavity field and with all the atoms initially in the ground state $|0\rangle$, the system can be described by the equations

$$\dot{a}=-[i(\Delta_{F1}-\Delta_{ac})+\gamma]a+ig\sqrt{N}\rho_{10}+G_{F1}^A\rho_{00}, \tag{1a}$$

$$\dot{\rho}_{10}=-(i\Delta_1+\Gamma_{10})\rho_{10}+ig\sqrt{N}a\rho_{00}+iG_2^{*}\rho_{20}, \tag{1b}$$

$$\dot{\rho}_{20}=-[i(\Delta_1+\Delta_2)+\Gamma_{20}]\rho_{20}+iG_2\rho_{10}, \tag{1c}$$

where a is the amplitude of the cavity field $\boldsymbol{E}_{F1}^A$, ρ_{ij} the density-matrix element, γ the cavity loss, g the single-atom-cavity coupling strength, N the number of atoms in the cavity, G_{F1}^A the Rabi frequency of $\boldsymbol{E}_{F1}^A$, $\Delta_{F1}=\Omega_1-\omega_{F1}$, and cavity frequency detuning $\Delta_{ac}=\Omega_1-\omega_c$ (with ω_c being the resonant frequency of the cavity). So, the amplitude of CTS is given by $a_{F1}=T_cG_{F1}^A\rho_{00}/\left\{[i(\Delta_{F1}-\Delta_{ac})+\gamma]+g^2N/\left(d_1+|G_2|^2/d_2\right)\right\}$, where T_c is the transmission function without dressing effect. The frequency ω_{F1} of the FWM signal is identical with ω_1 to obey the energy conservation, giving $\Delta_{F1}=\Delta_1$. According to the same coupled atom-cavity model, the CTS amplitude of $\boldsymbol{E}_S^A$ is given by $a_S=T_cG_S^A\rho_{00}/\left\{[i(\Delta_S-\Delta_{ac})+\gamma]+g^2N/\left(d_1+|G_2|^2/d_2+|G_3|^2/d_3\right)\right\}$.

1. Berman, P. R. *Cavity Quantum Electrodynamics* (Academic, New York, 1994).
2. Zhu, Y. *et al.* Vacuum Rabi splitting as a feature of linear-dispersion theory: Analysis and experimental observations. *Phys. Rev. Lett.* **64**, 2499–2502 (1990).
3. Thompson, R. J., Rempe, G. & Kimble, H. J. Observation of normal-mode splitting for an atom in an optical cavity. *Phys. Rev. Lett.* **68**, 1132–1135 (1992).
4. Klinner, J., Lindholdt, M., Nagorny, B. & Hemmerich, A. Normal mode splitting and mechanical effects of an optical lattice in a ring cavity. *Phys. Rev. Lett.* **96**, 023002 (2006).
5. Fleischhauer, M. & Lukin, M. D. Dark-state polaritons in electromagnetically induced transparency. *Phys. Rev. Lett.* **84**, 5094–5097 (2000).
6. Mucke, M. *et al.* Electromagnetically induced transparency with single atoms in a cavity. *Nature* **465**, 755 (2010).
7. Wu, H., Gea-Banacloche, J. & Xiao, M. Observation of intracavity electromagnetically induced transparency and polariton resonances in a Doppler-broadened medium. *Phys. Rev. Lett.* **100**, 173602 (2008).
8. Thompson, J. K., Simom, J., Loh, H. & Vuletić, V. A high-brightness source of narrowband, identical-photon pairs. *Science*, **313**, 74 (2006).
9. Wu, H. & Xiao, M. Bright correlated twin beams from an atomic ensemble in the optical cavity. *Phys. Rev. A* **80**, 063415 (2009).
10. Tanji-Suzuki, H. *et al.* Vacuum-induced transparency. *Science* **333**, 1266 (2011).
11. Kang, H., Hernandez, G. & Zhu, Y. Slow-light six-wave mixing at low light intensities. *Phys. Rev. Lett.* **93**, 073601 (2004).
12. Sevincli, S., Henkel, N., Ates, C. & Pohl, T. Nonlocal nonlinear optics in cold Rydberg gases. *Phys. Rev. Lett.* **107**, 153001 (2011).
13. Fleischhauer, M., Imamoglu, A. & Marangos, J. P. Electromagnetically induced transparency: Optics in coherent media. *Rev. Mod. Phys.* **77**, 633–673 (2005).
14. Zhang, Y. P., Brown, A. W. & Xiao, M. Opening four-wave mixing and six-wave mixing channels via dual electromagnetically induced transparency windows. *Phys. Rev. Lett.* **99**, 123603 (2007).
15. Zhang, Y. P., Khadka, U., Anderson, B. & Xiao, M. Temporal and spatial interference between four-wave mixing and six-wave mixing channels. *Phys. Rev. Lett.* **102**, 013601 (2009).
16. Boyer, V., Marino, A. M., Pooser, R. C. & Lett, P. D. Entangled images from four-wave mixing. *Science.* **321**, 544–547 (2008).
17. Corzo, N. V., Marino, A. M., Jones, K. M. & Lett, P. D. Noiseless optical amplifier operating on hundreds of spatial modes. *Phys. Rev. Lett.* **109**, 043602 (2012).
18. Zheng, H. *et al.* Parametric amplification and cascaded-nonlinearity processes in common atomic system. *Sci. Rep.* **3**, 1885 (2013).
19. Duan, L. M., Lukin, M. D., Cirac, J. I. & Zoller, P. Long-distance quantum communication with atomic ensembles and linear optics. *Nature*, **414**, 413 (2001).
20. Lukin, M. D., Fleishhauer, M., Scully, M. O. & Velichansky, V. L. Intracavity electromagnetically induced transparency. *Opt. Lett.* **23**, 295–297 (1998).
21. Wang, H., Goorskey, D., Burkett, W. H. & Xiao, M. Cavity-linewidth narrowing by means of electromagnetically induced transparency. *Opt. Lett.* **25**, 1732–1734 (2000).
22. Zhang, Y. P. *et al.* M. Evidence of Autler-Townes splitting in high-order nonlinear processes. *Opt. Lett.* **35**, 3420–2422 (2010).
23. Gea-Banacloche, J., Li, Y. Q., Jin, S. Z. & Xiao, M. Electromagnetically induced transparency in ladder-type inhomogeneously broadened media: Theory and experiment. *Phys. Rev A* **51**, 576 (1995).

Acknowledgments

This work was supported by the NBRPC (2012CB921804), NSFC (61205112, 61078002, 61078020, 11104214, 61108017, 11104216), and RFDP (20110201120005).

Author contributions

H.C. and Y.Z. wrote the main manuscript text and contributed to the theoretical and experimental analysis of this work. X.Y., Z.W. and X.Z. prepared figures 1–4. Y.Z. and M.X. provided the idea. All authors reviewed the manuscript.

Additional information

Competing financial interests: The authors declare no competing financial interests.

How to cite this article: Chen, H.X. *et al.* Parametrically Amplified Bright-state Polariton of Four- and Six-wave Mixing in an Optical Ring Cavity. *Sci. Rep.* **4**, 3619; DOI:10.1038/srep03619 (2014).